JOURNAL OF MATERIALS SCIENCE 32 (1997) 3727–3732

Effect of silicon ion implantation on the properties of a cast Co–Cr–Mo alloy

M. KAMIŃSKI, J. BASZKIEWICZ, J. KOZUBOWSKI, A. BEDNARSKA
Warsaw University of Technology, ul. Narbutta 85, 02-524 Warsaw, Poland

A. BARCZ
Institute of Electron Technology, Al. Lotników 46, 02-668 Warsaw, Poland

G. GAWLIK, J. JAGIELSKI
Institute of Electronics Materials Technology (IEMT), Wólczyńska 133, 01-919 Warsaw, Poland

The effect of silicon ion implantation upon the corrosion resistance and structure of the cast Co–Cr–Mo alloy of the Vitalium type, was examined. The silicon fluences were 1.5, 3.0 and $4.5 \times 10^{17} Si^+ cm^{-2}$. The surface layer of the Vitalium samples implanted with these silicon doses was found to become amorphous. Further annealing of the samples at 200 °C resulted in the $Cr_3Co_5Si_2$ phase being formed, whereas the amorphous layer was preserved. The Vitalium samples submerged in the 0.9% NaCl solution underwent mainly uniform corrosion, irrespective of whether or not they had been implanted with Si^+ ions. With increasing doses of implanted silicon and after annealing at 200 °C (samples implanted with $1.5 \times 10^{17} Si^+ cm^{-2}$), the corrosion resistance increased. The thickness of the oxide layer formed during the anodic polarization depended on the implanted silicon doses.

1. Introduction

Cobalt-based alloys belong to the group of metallic materials designed for use in osseous surgery [1, 2]. Their usefulness for medical purposes is due to their high biocompatibility when placed in the environment of human tissues and body fluids and also to their high resistance to pitting and crevice corrosion. They also show the ability to repassivate in physiological solutions. The presence of a metallic implant in the human body always involves the risk of inducing metallosis, i.e. the harmful effect upon the human body of the metal ions formed when the implant undergoes corrosion. Hence, it is extremely important that the number of metal ions that pass from the implant into the tissue that surround it should be reduced; this can be achieved by increasing the resistance of the implant to corrosion. One of the methods of improving the corrosion resistance of metal products is the implantation of various ions into their surface [3–7]. There are also reports on improving the corrosion resistance of alloy steels [8–11]. Both the literature [12–14] and our own experiments [15–17] suggest that one of the major effects that increase the corrosion resistance of implanted alloy steel is the transformation of the structure of its surface layer from the crystalline to the amorphous state. No reports have been found on the effects of the implantation of silicon ions into the surface of cobalt alloys on their corrosion resistance.

The aim of the present study was to examine how the corrosion resistance and structure of the surface layer formed on the Vitalium alloy depends on the fluence of the silicon ions implanted into it and on the post-implantation heat treatment. Silicon ions have been chosen for the implantation because no medical contra-indications are known [2].

2. Experimental procedure

The material examined was cast Co–Cr–Mo, whose determined chemical composition is given in Table I. The samples had the form of 14 mm diameter discs which were cut, using the electric spark method, from the hip joints delivered by the Hzwd Microhuta, Dąbrowa Górnicza, Poland. The samples were polished mechanically to obtain metallographic microsections, and then electrolytically at a temperature of 60 °C for 20s; the chemical composition of the bath was 96% glacial acetic acid, 4% water and $200 g dm^{-3}$ CrO_3.

The surfaces of the samples were implanted with silicon ions using the fluences 1.5×10^{17}, 3.0×10^{17} and $4.5 \times 10^{17} Si^+ cm^{-2}$. The energy of the ion beam was 100 keV and the electric current ranged from 1–1.5 $\mu A cm^{-2}$. During implantation, the temperature of the samples did not exceed 70 °C. The process was carried out using a Balzers MPB-202RP implanter at the laboratory of the IEMT. Some of the samples implanted with $1.5 \times 10^{17} Si^+ cm^{-2}$ were then annealed at 200 °C in vacuum (10^{-6} torr) for 1 h. The corrosion resistance was measured in a non-deaerated

0022–2461 © 1997 Chapman & Hall

TABLE I The chemical composition of the Co–Cr–Mo alloy (wt %)

C	P	S	Mn	Si	Cr	Ni	Mo	Fe	Co
0.35	0.04	0.011	0.65	0.76	29.4	0.12	6.1	3.9	Bal.

0.9% NaCl solution at a temperature of 37 °C. Prior to the measurement, the samples were exposed to the measurement environment for 24 h so that the corrosion potential could stabilize. The measurements were made using the potentiodynamic method, by changing the polarization of the samples from the corrosion potential towards positive potentials at a rate of $1\,mV\,s^{-1}$, until the current reached a few milliamps. The potential at which the anodic current reaches a value of $1\,\mu A\,cm^{-2}$ is denoted E_{wp}. At this potential, the anodic polarization curve shows a relatively rapid increase of the anodic current. From the polarization curves obtained, we determined the electric charge that passed through the sample surfaces when the potential was increased from 0 V to 1 V. After these measurements, the samples were examined in an optical microscope and a scanning electron microscope. In addition to the polarization curves, the polarization resistances were determined using the Stern method [18, 19]. The reference electrode was a saturated calomel electrode.

The structural examinations were performed with a Philips EM300 electron microscope. The samples were cut by the electric spark method and then thinned at their un-implanted sides until a perforation occurred. The samples examined included those implanted with silicon with fluences of 1.5×10^{17} and $4.5 \times 10^{17}\,Si^{+}\,cm^{-2}$, non-implanted samples, and a number of the $1.5 \times 10^{17}\,Si^{+}\,cm^{-2}$ implanted samples annealed at a temperature of 200 °C.

The chemical composition profiles of the implanted samples before and after the corrosion measurements were determined using secondary ion spectrometry (SIMS) with an Ar^{+} ion beam of energy of 4 keV. The scanned area was about $1\,mm^2$. The material was removed at a rate of about $0.15\,nm\,s^{-1}$.

3. Results

The TEM results show that the process of silicon ion implantation into the Vitalium alloy results in the alloy surface becoming amorphous. In the initial state, the surface layer has a structure characteristic of a polycrystalline material. It contains large grains with a low dislocation density and grain boundaries with visible precipitates. After the implantation with silicon ion doses of 1.5 and $4.5 \times 10^{17}\,Si^{+}\,cm^{-2}$, the layer appeared to be amorphous. Fig. 1 shows the diffraction pattern obtained from a very thin region, and an image of the surface structure obtained for the sample implanted with $1.5 \times 10^{17}\,Si^{+}\,cm^{-2}$. When a sample implanted with this dose is annealed at a temperature of 200 °C, the silicide phase appears in the form of elongated plates coherent with the matrix (Fig. 2a),

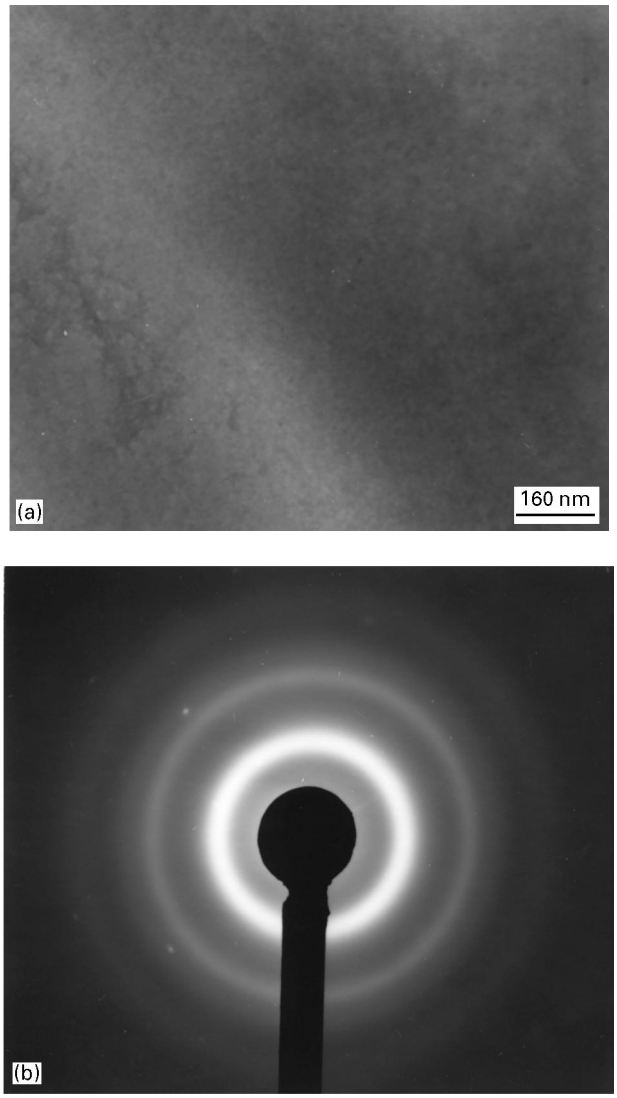

Figure 1 (a) Microstructure and (b) diffraction pattern of silicon-implanted Co–Cr–Mo alloy for the dose of $1.5 \times 10^{17} Si^{+}\,cm^{-2}$.

which suggests that the crystallization nuclei form in contact with the matrix. In the figure, we can see three different families of these elongated plates. Fig. 2b shows their complex diffraction pattern. Diffraction pattern gives d values of 0.42, 0.219, 0.196, 0.118 nm, corresponding to the spots close to the centre; d values for $Cr_3Co_5Si_2$ phase, cubic $a = 0.8704$ nm (JCDD PDS2 Nr 16–35) are 0.435 nm (not indicated on the PDS card, but calculated as d_{200}) and 0.2179, 0.2049, … ,0.1184 nm; better fit is obtained by assuming tetragonal distortion ($a = 0.876$ nm, $c = 0.84$ nm). The diffraction pattern of Fig. 2b also shows that the annealing of the implanted Vitalium at 200 °C does not lead to the complete disappearance of the amorphous phase.

Examples of the anodic polarization curves for various silicon ion doses obtained from the electrochemical measurements are shown in Fig. 3. Fig. 4 shows how the annealing at 200 °C affects the shape of the polarization curves. Figs 5 and 6 are scanning electron micrographs of the sample surfaces: Fig. 5 shows an implanted surface prior to the electrochemical measurements, and Fig. 6 the damage due to corrosion after the complete anodic polarization curve

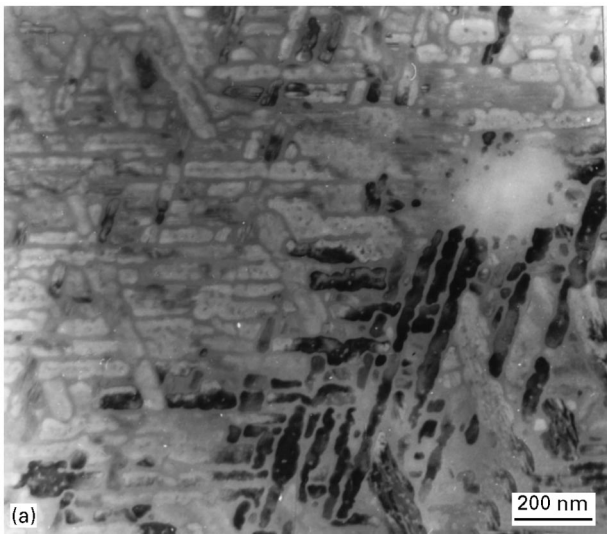

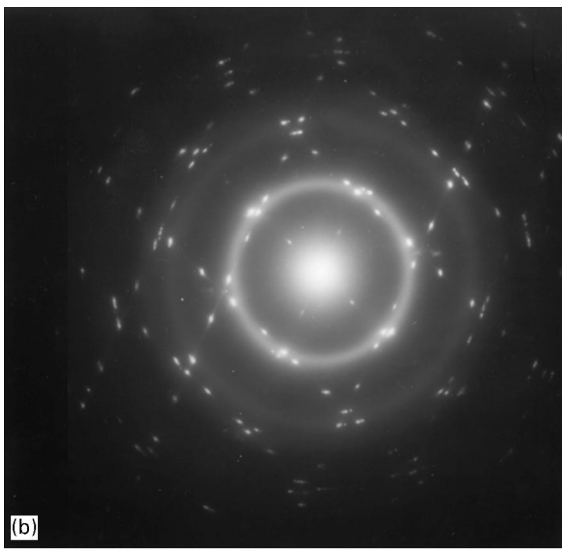

Figure 2 (a) Microstructure and (b) diffraction pattern of silicon-implanted Co–Cr–Mo alloy for the dose of $1.5 \times 10^{17}Si^{+}\ cm^{-2}$. After implantation, specimens were annealed 1 h at 200 °C.

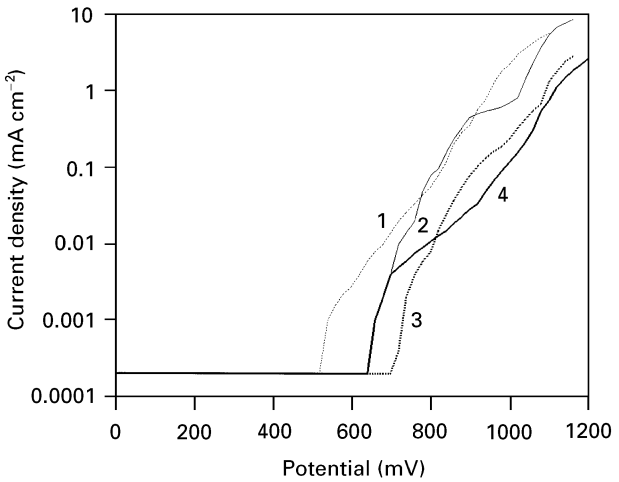

Figure 3 The anodic polarization curves measured for the Co–Cr–Mo alloy in a solution of 0.9% NaCl. (1) Un-implanted specimen, (2) specimen implanted with a $1.5 \times 10^{17}Si^{+}\ cm^{-2}$ dose, (3) specimen implanted with a $3 \times 10^{17}Si^{+}\ cm^{-2}$ dose, (4) specimen implanted with a $3 \times 10^{17}Si^{+}\ cm^{-2}$ dose.

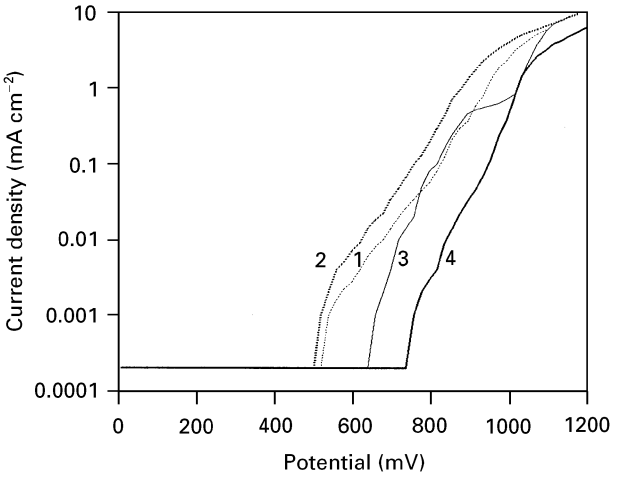

Figure 4 The anodic polarization curves measured for the Co–Cr–Mo alloy in a solution of 0.9% NaCl. (1) Un-implanted specimen, (2) un-implanted specimen, annealed 1 h at 200 °C (3) specimen implanted with a $1.5 \times 10^{17}Si^{+}\ cm^{-2}$ dose, (4) specimen implanted with a $1.5 \times 10^{17}Si^{+}\ cm^{-2}$ dose, annealed 1 h at 200 °C.

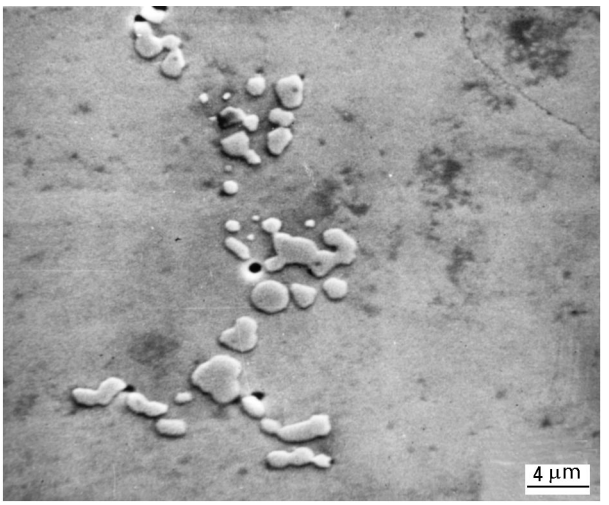

Figure 5 SEM image of the surface of the specimen implanted with a $1.5 \times 10^{17}Si^{+}cm^{-2}$ dose before the anodic polarization.

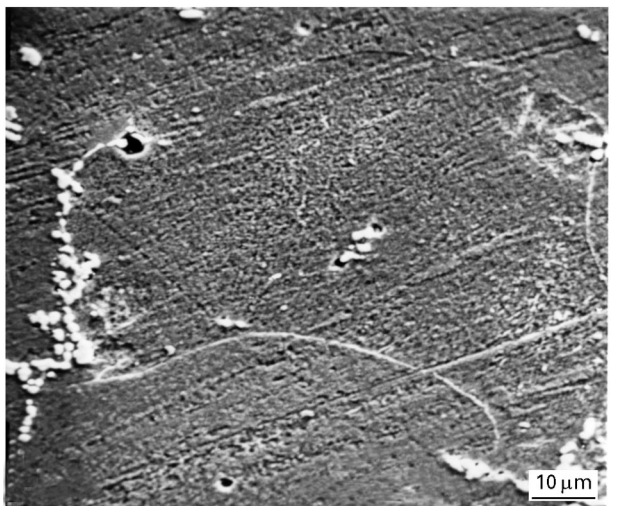

Figure 6 SEM image of the surface of the specimen implanted with a $1.5 \times 10^{17}Si^{+}cm^{-2}$ dose after the anodic polarization.

TABLE II Results of electrochemical experiments

Dose ($10^{17}Si^+ cm^{-2}$)	E_{corr} (mV)	R_{pol} ($M\Omega\,cm^2$)	E_{wp} (mV)	Q_{anod} ($mC\,cm^{-2}$)	i_{corr} ($nA\,cm^{-2}$)	V_p ($nm\,y^{-1}$)
Un-implanted	196	4	540	139	21.64	234
Un-implanted[a]	9	1.8	500	325	47.80	517
1.5	106	11.6	660	83	7.47	81
1.5[a]	131	45.6	760	15	1.97	21
3	142	17.2	720	20	5.06	55
4.5	180	17.2	660	10	5.06	55

[a] Specimens were annealed for 1 h at 200 °C.

in a 0.9% NaCl solution is taken. The results obtained from the electrochemical measurements by the Stern method and from the anodic polarization curves are given in Table II. The values of the corrosion current density, i_{corr}, have been calculated assuming that the slope of the Tafel region of the cathodic straight line is 200 mV per current decade. The corrosion rate, V_p, was calculated by assuming that the metal which undergoes dissolution is cobalt.

The shapes of all the anodic curves are similar (Figs 3 and 4): within a wide potential range (from E_{corr} to about 500 mV) the anodic current density is very small ($0.2\,\mu A\,cm^{-2}$). Hence we can conclude that the alloy examined is in the passive state. Moreover, no current loops characteristic of pitting corrosion are observed after the polarization direction is reversed. This suggests that pitting corrosion is not a dominant type of corrosion. Small and sparse pores visible at the polarized surface (Fig. 6) are present already in the implanted material before polarization (Fig. 5). The process of corrosion seems to proceed through grain and/or phase boundaries [20, 21]. During the measurement, the samples are uniformly dissolved with simultaneous formation of an oxide film. The values of the polarization resistances suggest that the silicon ion implantation results in an increase of the corrosion resistance of the alloy. After annealing, the polarization resistance of the $1.5 \times 10^{17} Si^+ cm^{-2}$ implanted samples increased 11-fold when compared with the samples that were not implanted.

The silicon ion implantation affects the values of the potential E_{wp} only slightly. The greatest increase of this potential (about 220 mV) is observed in the samples that, after implantation, have been subjected to annealing (Fig. 4).

Another parameter measured in order to evaluate how silicon ion implantation into the surface of the Vitalium alloy affects the corrosion resistance, is the electric charge, Q_{anod}, which flows through the sample surface during its polarization from the corrosion potential to a potential of + 1 V. Because no oxygen in the gaseous phase was observed to evolve during the entire measurement, we assumed that the amount of this charge is determined by the rate of anodic dissolution of the alloy and the formation of the oxide film during the polarization process. If so, the greater the charge Q_{anod}, the smaller should be the corrosion resistance of the alloy. As can be seen from Table II, the implantation process reduces the total charge density by more than a factor of ten (compare the results obtained for the $4.5 \times 10^{17} Si^+ cm^{-2}$ implanted sample and for the non-implanted sample).

Silicon profiles, calculated with TRIM code [22] are presented in Fig. 7. The concentrations of cobalt, silicon and oxygen in the surface layers of all the samples were examined before and after the electrochemical measurements by the SIMS technique. Fig. 8 gives the results obtained for samples implanted with 1.5, 3.0 and $4.5 \times 10^{17} Si^+ cm^{-2}$. Analysis of the chemical compositions of the implanted layers show that the depth to which the signal due to silicon is significant is about 150–170 nm, and that, practically, this depth does not depend on the silicon dose. As the silicon dose increases, the signal representing the presence of silicon in the implanted layer increases (from 2×10^3 at a dose of $1.5 \times 10^{17} Si^+ cm^{-2}$ to 8×10^3 at a dose of $4.5 \times 10^{17} Si^+ cm^{-2}$), whereas the silicon concentration profile changes only slightly. For doses of 1.5 and $3.0 \times 10^{17} Si^+ cm^{-2}$, the silicon concentration profiles show blurred maxima at mid-thickness of the implanted layer. In samples implanted with $4.5 \times 10^{17} Si^+ cm^{-2}$, on the other hand, a broad plateau occurs (Fig. 8e), which might suggest that the

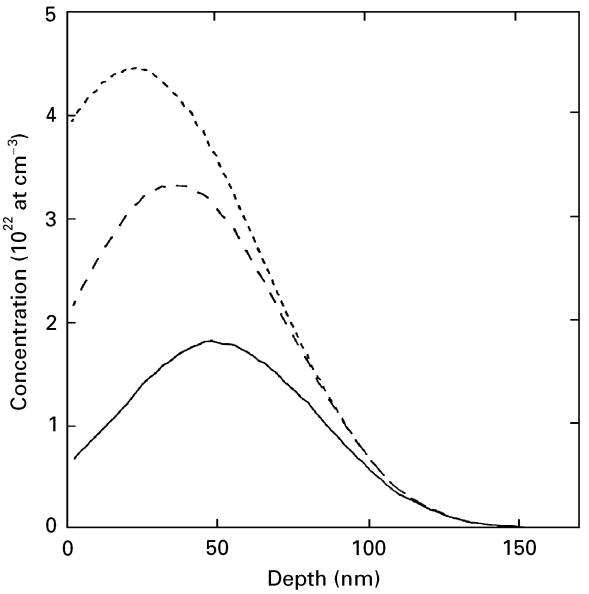

Figure 7 The concentration profiles calculated for the applied ion fluences. "TRIM-92" code was used for calculation. (——) 1.5×10^{17} at cm^{-2}, (– – –) 3×10^{17} at cm^{-2}, (- - -) 4.5×10^{17} at cm^{-2}.

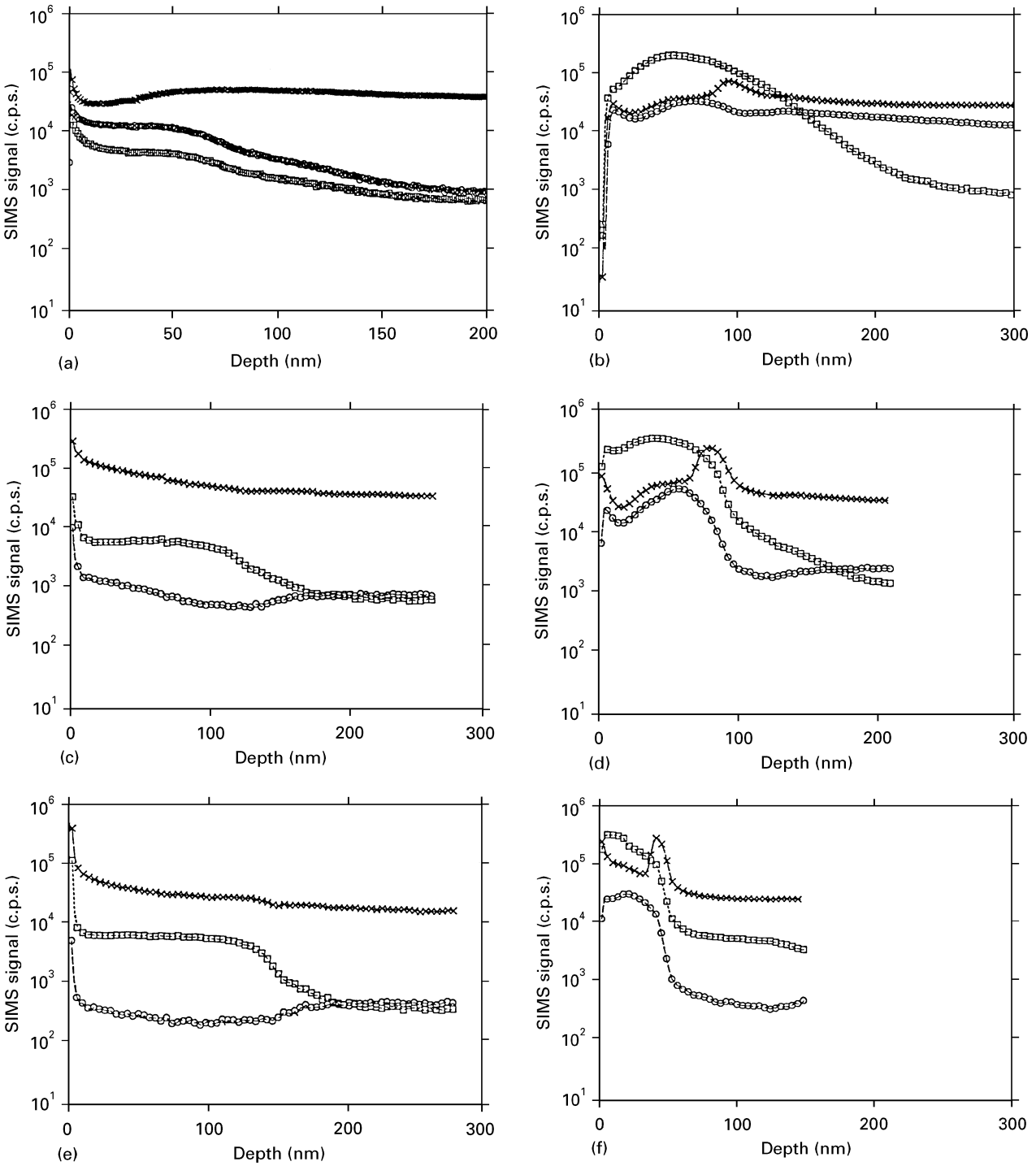

Figure 8 Silicon, oxygen and cobalt concentration depth profiles. (a) Un-implanted specimen after anodic polarization, (b) silicon dose $1.5 \times 10^{17} Si^{+} cm^{-2}$, annealed 1 h at 200 °C, after anodic polarization, (c) silicon dose $3 \times 10^{17} Si^{+} cm^{-2}$, before the anodic polarization, (d) silicon dose $3 \times 10^{17} Si^{+} cm^{-2}$, after the anodic polarization, (e) silicon dose $4.5 \times 10^{17} Si^{+} cm^{-2}$, before the anodic polarization, (f) silicon dose $4.5 \times 10^{17} Si^{+} cm^{-2}$, after the anodic polarization. (x) Cobalt, (□) silicon, (○) oxygen.

alloy constituents form chemical bonds with silicon (compare to Fig. 7). Diffraction patterns (taken during TEM studies of the surface layer) did not, however, show the presence of a new phase.

In $1.5 \times 10^{17} Si^{+} cm^{-2}$ implanted samples, the silicon concentration profile remains unchanged after post-implantation annealing at 200 °C for 1 h. The electrochemical measurements, on the other hand, significantly affect the concentration profiles of all the elements examined. The thicknesses of the affected surface layer is about 120 nm.

The changes in the oxygen concentration profiles indicate that oxide films have formed on the sample surfaces; the thickness of these films depends on the implanted silicon dose and on the heat treatment applied. The thinnest (about 50 nm, Fig. 8f) oxide film forms on the samples implanted with $4.5 \times 10^{17} Si^{+} cm^{-2}$. In those implanted with the $3.0 \times 10^{17} Si^{+} cm^{-2}$ dose, the thickness of the oxide film increases to 100 nm (Fig. 8d), and with the $1.5 \times 10^{17} Si^{+} cm^{-2}$ dose (in samples subjected to annealing) it increases to 130 nm (Fig. 8b). The oxide film forming on the un-

implanted samples during the electrochemical measurements has been estimated to be 150 nm thick (Fig. 8a). The SIMS results are in good agreement with the amount of electric charge (determined from the anodic polarization curves) that flowed through the sample surface during the polarization (Table II), but this agreement does not apply to the samples annealed after polarization. The samples subjected to annealing showed the greatest increase of the corrosion resistance, which can perhaps be attributed to the formation of the $Cr_3Co_5Si_2$ phase during the annealing and formation of protective oxide films during the electrochemical measurements.

Fig. 8b, d and f show an increase of the cobalt signal at the oxide phase/alloy interface. This can be explained by the oxidation of cobalt which then dissolves in the electrolyte and, thus, its concentration in the surface layer decreases. Such an effect is not observed in non-implanted samples and in samples implanted with the smallest silicon dose, where the oxide films are thicker.

The increased concentration of silicon observed after polarization can be attributed to both its oxidation and the reduction in the concentrations of the other constituents of the alloy. The layer formed during the anodic polarization is rich in silicon and oxygen – it is certainly silicon dioxide. Most probably, it is this layer which is responsible for the increase in the corrosion resistance of the alloy.

4. Discussion and conclusions

It is difficult to determine precisely how the corrosion resistance of cobalt alloys increases after the implantation, because, even unmodified, they show a high resistance to corrosion. To estimate the effect of implantation, more than one criterion should be considered. This is why, based on the results of electrochemical measurements we also determined the values of the polarization resistance, R_p (by the Stern method), and hence, indirectly, the corrosion current densities for the individual types of the samples examined. Because the dominant kind of damage due to corrosions here is uniform corrosion, we could calculate the corrosion rate expressed in nm year^{-1}. The results are shown in Table II. They show that the implantation reduces the corrosion rate several times compared to that observed in the non-implanted material.

The major conclusions from this investigation are as follows.

1. In cobalt alloys of the Vitalium type submerged in 0.9% NaCl solution, the predominant type of damage due to corrosion is slow uniform corrosion.

2. The implantation of silicon ions into the Vitalium surface increases its corrosion resistance, which can be seen from the increased polarization resistance, increased potential, E_{wp}, and reduced amount of the electric charge which flows when the sample is subjected to polarization from the corrosion potential to a potential of 1 V.

3. As a result of the implantation, the surface layer becomes amorphous, which may be one of the factors contributing to the increased corrosion resistance.

4. As the silicon fluence is increased, the corrosion resistance of the alloy increases; the optimum fluence appears to be $3.0 \times 10^{17} Si^+ cm^{-2}$.

5. When the implanted cobalt alloys are subjected to annealing, the $Cr_3CO_5Si_2$ phase is formed, visible on the background of the amorphous structure. The corrosion resistance then increases considerably compared with that of unannealed material.

Acknowledgement

This work was supported by the Committee for Scientific Research of Poland through Grant 3 P 40705104.

References

1. H. S. DOBBS and J. L. M. ROBERTSON, *J. Mater. Sci.* **18** (1983) 391.
2. J. MARCINIAK, "Biomateriały w Chirurgii Kostnej" (Wyd. Pol. Śląskiej, Gliwice, 1992).
3. H. J. KIM, W. B. CARTER, R. F. HOCHMAN, E. L. MELETIS, G. K. WOLLF, W. A. GRANT and R. P. M. PROCTER, *Mater. Sci. Eng.* **69** (1985) 297.
4. C. R. CLAYTON, K. G. K. DOSS, Y-F. WANG, J. B. WARREN, G. K. HUBLER, in "Proceedings of the 3rd International Conference on Modification of Surface Properties of Metals by Ion Implantation", edited by V. Ashworth, W. A. Grant, R. P. M. Procter (Pergamon Press, 1981) p. 67.
5. J. GŁUSZEK, J. JĘDRKOWIAK, J. MARTIN and J. MASALSKI, *Ochrona przed korozją* **30** (1987) 77.
6. S. B. AGARWAL, Y. WANG, C. R. CLAYTON and H. HERMAN, *Thin Solid Films* **63** (1979) 19.
7. MASAYA IWAKI, *Mater. Sci. Eng.* **69** (1985) 211.
8. E. JOHNSON, A. JOHNSON and L. SARHOLT-KRISTENSEN, *Nucl. Instrum. Meth. Phys. Res.* **B4**/**8** (1985) 212.
9. Y. F. WANG, C. R. CLAYTON, G. K. HUBLER, W. H. LUCKE and J. K. HIRVONEN, *Thin Solid Films* **63** (1979) 11.
10. Q. M. ChEN, H. M. ChEN, X. D. BAI, J. Z. ZHANG and H. H. WANG, *Nucl. Instrum. Meth.* **209** (1983) 867.
11. H. J. KIM, W. B. CARTER, R. F. HOCHMAN, E. L. MELETIS, G. K. WOLF, W. A. GRANT and R. P. M. PROCTER, *Mater. Sci. Eng.* **69** (1985) 2976.
12. P. MUN and G. K. WOLF, *Nucl. Instrum. Meth.* **7**–**8** (1985) 205.
13. E. C. COONEY and D. I. POTTER, *Surf. Coat. Technol.* **51** (1992) 420.
14. P. ZIEMANN, *Mater. Sci. Eng.* **69** (1985) 95.
15. J. BASZKIEWICZ, M. KAMIŃSKI, A. PODGÓRSKI, J. JAGIELSKI and G. GAWLIK, *Corros. Sci.* **5** (1992) 15.
16. J. BASZKIEWICZ, M. KAMIŃSKI, D. KRUPA, J. KOZUBOWSKI, E. JEZIERSKA, G. GAWLIK, J. JAGIELSKI and J. BARCZ, Materialy IV Krajowej Konferencji Korozyjnej "Korozja'93", Warsaw, Poland (Institute of Physical Chemistry, Polish Academy of Science, Warsaw, 1993) p. 317.
17. M. KAMIŃSKI, J. BASZKIEWICZ and D. KRUPA, *Ochrona przed korozja* **5** (1995) 105.
18. M. STERN and A. L. GEARY, *J. Electrochem. Soc.* **104** (1957) 56.
19. M. STERN and E. D. WEISERT, "Experimental Observations on the Relation between Polarization Resistance and Corrosion Rate" in ASTM Proceedings, Vol. 59 (American Society for Testing and Materials, Philadelphia, PA, 1959) p. 1280.
20. B. C. SYRETT and S. S. WING, *Corros. NACE* **34** (4) (1978) 138.
21. E. ANGELINI and F. ZUCCHI *J. Mater. Sci. Mater. Med.* **2** (1991) 27.
22. J. F. ZIEGLER and J. P. BIERSACK, "The Stopping and Range of Ions in Solids" (Pergamon Press, New York, 1985) Software "TRIM-92".

Received 23 February 1996
and accepted 28 January 1997